ELECTRICAL ENGINEERING AND ENERGY

OPEN ACCESS

A Comparative Study of Wavelet and EMD Methods for Radar-Based Detection of Rotational Imbalance in Induction Motors

Yunus Emre Acar[1]

[1] Dept. of Electrical and Electronics Engineering, Selçuk University, Konya, Türkiye

Submitted : 15 August 2025
Accepted : 29 August 2025
Online First: 31 August 2025

Corresponding author
Yunus Emre Acar,
yacar@selcuk.edu.tr

DOI:10.64470/elene.2025.1007

Abstract: This paper presents a radar-based methodology for detecting rotational imbalance in machinery. The approach employs multi-resolution signal processing techniques, specifically comparing Empirical Mode Decomposition (EMD) and Wavelet Decomposition (WD), for feature extraction from radar-acquired signals. Both methods generated five levels of sub-components. Time-domain features were extracted individually from each sub-component, and the resultant feature vectors from all levels were concatenated to form the final input for machine learning classifiers. WD was evaluated using three distinct mother wavelet functions (Haar, Coiflet-2, and Symlet-4), with the performance of each benchmarked against EMD. The comparative analysis rigorously assessed classification metrics (accuracy, precision, recall, F1-score) alongside computational efficiency metrics (model size, training and prediction latency). Results demonstrate that wavelet-derived features consistently outperformed EMD across all classifiers. The Haar-Random Forest combination achieved the highest classification accuracy (95.28%). Support Vector Machines paired with Haar features offered an optimal accuracy-latency trade-off (approximately 219 ms training time), while Decision Trees delivered ultra-fast inference (0.6 ms). These findings validate the practical viability and effectiveness of the proposed radar-based vibration detection framework for industrial condition monitoring systems.

Keywords Empirical Mode Decomposition (EMD), Machine Learning (ML), Multi-Resolution Analysis (MRA), Radar-Based Monitoring, Rotational Imbalance Detection, Wavelet Decomposition (WD).

1. Introduction

Vibration analysis represents a critical research domain for health monitoring, fault detection, and performance evaluation of engineering systems (Matania et al., 2024). In industrial applications, vibration monitoring systems are extensively deployed across diverse areas, including rotating machinery, bridges, buildings, and aerospace systems (Kiliç & Acar, 2024; Vaishnavi et al., 2025; Ye et al., 2022). Particularly in rotational systems, which have limitations due to primary friction forces (Yücel et al., 2025), the early detection of mechanical faults such as imbalance, bearing defects, and gearbox issues is vital for preventing unexpected downtime and minimizing maintenance costs (Seid Ahmed et al., 2025; Tama et al., 2023).
Although traditional condition monitoring techniques have provided valuable insights for industrial

diagnostics, each method faces significant operational challenges. Contact-based vibration sensors, for instance, can introduce mass-loading effects and often require invasive installation procedures, problematic in hazardous environments (Kiranyaz et al., 2024). Acoustic approaches are highly susceptible to interference from ambient noise, demanding sophisticated denoising strategies to ensure reliable results (Glowacz et al., 2025). Electrical current signature analysis lacks sensitivity to mechanical faults and is prone to electromagnetic interference (Jiang et al., 2019).

Differing from conventional approaches, radar-based vibration sensing effectively overcomes the key drawbacks of traditional methods: it eliminates the mass-loading and invasive installation issues associated with contact sensors, avoids the susceptibility to ambient noise that limits acoustic techniques, and is immune to the electromagnetic interference that affects current-based analysis. Recent advancements have highlighted the precision and versatility of radar technology. Wen et al. achieved micron-level radar-based vibration measurements with high signal-to-noise ratios using their proposed DeepVib deep learning algorithm (Wen et al., 2024). In a study conducted by Acar and Çetinkal, bearing defects across 15 different damaged bearing datasets were classified with high accuracy by monitoring the vibration of motors with faulty bearings (Acar & Çetinkal, 2025). Ren et al. implemented high-precision three-dimensional vibration measurements utilizing three different Frequency-Modulated CW radars (Ren et al., 2023).

Whether employing conventional or modern technologies, extracting meaningful information from vibration signals necessitates a series of signal processing steps. While traditional Fourier transform-based spectral analysis methods constitute fundamental approaches, time-frequency transformations are widely utilized for time-frequency analysis (Bolshakova et al., 2023; Manhertz & Bereczky, 2021; Wu & Yang, 2025). However, the typical non-linear and non-stationary characteristics of vibration signals have increased the demand for adaptive signal decomposition methods.

Empirical Mode Decomposition (EMD) offers adaptive and localized analysis by decomposing non-stationary signals into Intrinsic Mode Functions (IMFs), thereby extracting different resolutions directly from the data itself without relying on fixed functions or filters (Jaarsveldt et al., 2023; Şeflek, 2025). Li et al. (Li et al., 2023) tested various EMD variants in industrial vibration analysis and proposed a variant that outperforms existing ones. Although conventional EMD has proven effective in analyzing non-stationary data, Stallone et al. demonstrated that improper applications are inevitable if its fundamental constraints are not considered (Stallone et al., 2020). One of the most critical disadvantages of EMD is the mode mixing problem, which occurs when similar frequency components are distributed across different IMFs or when signals of different scales mix within the same IMF. Wavelet transformation, however, offers a significant alternative by using predefined mother wavelet functions that are unaffected by mode mixing problems and provide consistent time-frequency localization (Ganguly et al., 2022; Guo et al., 2022). Due to its stable structure, Wavelet Decomposition (WD) has been the subject of numerous studies in detecting mechanical faults such as bearing and gearbox defects (Han et al., 2022; Jiang et al., 2020; Zheng et al., 2024).

Despite the widespread use of EMD and wavelet-based approaches in conventional sensor-based vibration analysis, studies systematically examining the performance of these methods with radar-acquired vibration data remain considerably limited. The primary objective of this study is to comprehensively investigate the performance of EMD and WD methods in radar-based vibration detection systems. Within the scope of this work, the imbalance problem in rotational systems was selected as a realistic and industrial test scenario, and the performance of the methods was compared through experimental studies.

This study contributes to the literature in the following aspects:

- Systematic comparison and parameter optimization of EMD and WD methods for feature extraction in radar-detected vibration signals.
- Parametric comparison of different machine learning algorithms' performance on radar-based vibration data and determination of optimal classification strategies.

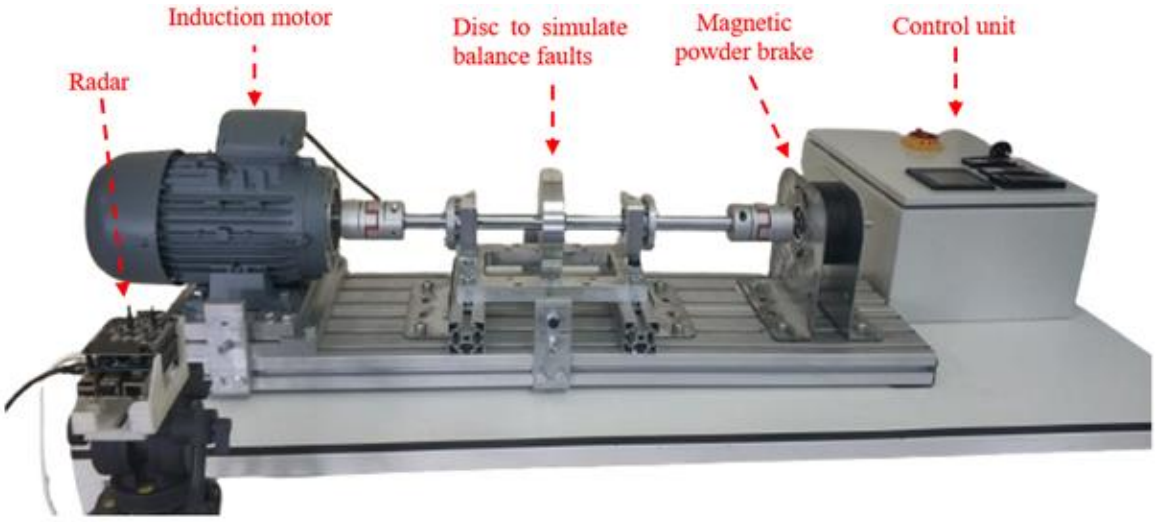

Figure 1 The experimental test setup

To ensure a comprehensive evaluation of the feature extraction methods, our analysis incorporates a systematic comparison of classification performance using multiple machine learning algorithms —Support Vector Machine (SVM), k-Nearest Neighbors (KNN), Random Forest (RF), and Decision Tree (DT) — with parameter optimization through grid search, considering both classification accuracy and computational efficiency metrics relevant to industrial applications.

The organization of the subsequent sections of this paper is as follows: The second section details the experimental setup, data collection procedure, and applied signal processing methods. The third section presents the experimental results and comparative analyses in detail. Finally, the fifth section assesses the study and recommendations for future research.

2. Materials and Methods

In this study, a dataset was created for imbalance detection in rotational systems using a 24 GHz CW radar system based on Raspberry Pi 4. The experiments aimed to detect imbalances created with an asynchronous motor fault simulation test set designed by Piritech Electric Vehicle and Automation Systems (n.d.). Three different levels of imbalanced rotation were achieved by placing weights of varying mass on a metal disc driven by an asynchronous motor. A radar module directed at the motor housing from the radial axis was utilized to obtain baseband signals modulated by motor vibration. Quadrature radar signals received through RF Beam's KLC5 module were amplified by approximately 40 dB using identical active Butterworth filters and filtered within the range of 0.01-1.6 KHz. The signals were digitized at a 10 KHz sampling rate using an MCC118 Daq Hat and processed offline. Figure 1 shows the data collection system. Table 1 presents the list of primary components in the experimental setup.

Table 1 List of primary components in the experimental setup

Component	Specifications	Explanation
Volt VM 90S-4 Induction motor	1.1 kW, 1500 rpm, 3-phase	rotates the coupled disc
ABB ACS150-01E-07A5-2 motor driver	50/60 Hz, 220V, 1.5 kW	controls the motor speed
EMF ABTF02 magnetic powder brake	15 Nm, 24 W, 24 V_{in}	load for the motor
EMF TFD-02 mag. powder brake driver	12-48 VDC, operation options (4-20 mA, 0-10V, Potentiometer, Modbus)	drives the load

2.1 Dataset Generation

The KLC5 module is a 24 GHz homodyne radar transceiver with IQ demodulation providing dual-channel I and Q analog signals. These signals, modulated by target movement, contain information about target displacement. For micro-level displacements, the phase of the signal is extracted using methods such as arctangent transformation, complex signal demodulation, DACM, and EDACM. This phase signal contains displacement information. In this study, a complex-valued signal was formed using I and Q signals with a 90-degree phase difference as shown in Equation (1).

$$x(t) = i(t) + jq(t) \tag{1}$$

The spectrum of this complex-valued signal is rich in information content as it provides both the frequency of target movement and directional information. In this study, the phase and amplitude of the complex-valued signal were calculated as shown in Equations (2.a) and (2.b) and used together.

$$phase(t) = arctan2\left(\frac{q(t)}{i(t)}\right) \tag{2.a}$$

$$amp(t) = \sqrt{i^2(t) + q^2(t)} \tag{2.b}$$

Here, the arctan2 function is a two-argument arctangent function that returns the angle in the correct quadrant based on the signs of both input arguments, providing a full 360-degree range of values.

In each of the 1,802 separate experiments conducted, phase and amplitude signals of length 30,000 were generated (30-second and 10 kHz sampling rate). The experiments include data for four different levels of imbalance: a baseline class created without attaching any disc to the disc rotated by the motor, a mild imbalance class created by attaching 10 g to the disc, a moderate imbalance class created by attaching 20 g, and a severe imbalance class created by attaching 30 g. Data were diversified through experiments conducted at different times, speeds, and loads. Table 2 summarizes the basic information about the dataset. The dataset has been shared on the KAGGLE platform with open access (Acar, 2025).

Table 2 Dataset Characteristics

Parameters	Values
RPM	{500, 600, …,1400, 1500}
Weights (source of imbalance)	{0 g, 10 g, 20 g, 30 g}
Load (mag. pow. brake)	{0, 0.6, 1.2, 1.8, 2.4, 3}
# of experiments per classes	{462, 464, 413, 463}

These signals were decomposed into different frequency bands using approaches such as EMD and WD. The sub-frequency components obtained after these approaches were subjected to time-domain feature extraction to form the input to the classifier.

2.2 Empirical Mode Decomposition (EMD)

EMD is a data-driven method developed for the self-adaptive decomposition of non-linear and non-stationary signals Huang et al., 1998. Unlike transformations such as the wavelet transform, this method does not use a selected basis function. Instead, it uses the signal's internal oscillations, thus practically obtaining the concept of instantaneous frequency.

In this decomposition method, the signal $x(t)$ is modeled as the sum of K intrinsic mode components $IMF_k(t)$ with a residual signal $r_K(t)$ as given in Equation (3).

$$x(t) = \sum_{k=1}^{K} IMF_k(t) + r_K(t), \quad K < \infty \tag{3}$$

In the EMD algorithm, there are two fundamental conditions that the $IMF_k(t)$ components must satisfy. Let n_0 be the number of zero-crossing points of the signal and n_e be the number of local extrema, then $|n_0 - n_e| \leq 1$ must hold. Additionally, for each moment t, the mean of the upper and lower envelopes of the signal $m(t)$ must oscillate around zero as given in Equation (4).

$$m(t) = \frac{e_u(t) + e_l(t)}{2} \approx 0 \tag{4}$$

Here, $e_u(t)$ and $e_l(t)$ represent the upper and lower envelopes of the signal, respectively. In EMD, which is an iterative process, first, the mean signal $m(t)$ is obtained from the $e_u(t)$ and $e_l(t)$ envelope signals passing through the local maximum and minimum points of the input signal $x(t)$. The high-frequency detail signal $h(t)$ is obtained as the difference between $x(t)$ and $m(t)$, as given in Equation (5).

$$h_1(t) = x(t) - m(t) \tag{5}$$

If this detail signal $h(t)$ does not satisfy the conditions for being an IMF component, the mean of its envelopes is calculated, and a similar difference signal is obtained. The process continues iteratively until the resulting difference signal satisfies the conditions. Additionally, the filtering process is terminated when the energy ratio between two consecutive detail signals obtained in each iteration falls below a certain threshold value (typically 0.2). The difference signal that satisfies the conditions at the nth iteration is assigned as the first IMF component $IMF_1(t)$, and the first-level residual signal $r_1(t)$ is obtained as given in Equation (6).

$$r_1(t) = x(t) - IMF_1(t) \tag{6}$$

By considering the first-level residual signal as the initial input signal and repeating the entire process, the second-level IMF component is obtained. This process continues until the maximum IMF component is found or until the residual signal becomes monotonic. The pseudocode of the algorithm can be summarized as shown in Figure 2.

1) Initialization: Start with the raw signal $x(t)$ as the initial residue.
2) Sifting Loop: For each residue:
    i. Identify local maxima/minima to construct upper/lower $(e_u(t), e_l(t))$ envelopes.
    ii. Compute the mean envelope $m(t)$ (Eq. 4).
    iii. Extract the detail $h(t) = residue - m(t)$ (Eq. 5).
    iv. Repeat sifting until h(t) satisfies IMF conditions
3) Termination: Stop when residue becomes monotonic or reaches maximum IMFs.

Figure 2 Pseudocode of the EMD algorithm

2.3 Wavelet Decomposition (WD)

The Wavelet transform is a powerful signal processing method that enables localization of a signal in both time and frequency domains, exhibiting superior performance, particularly in the analysis of transient and sudden changes (Acar et al., 2019) . The selection of the mother wavelet function (such as Haar, Daubechies, Symlet) allows optimization of time-frequency resolution according to the characteristics of the analyzed signal. One of the most critical advantages of WD is its ability to detect transient and sudden changes in the signal with high precision and to reconstruct the original signal losslessly. Additionally, it offers a structure more resistant to problems such as mode mixing and is preferred in applications like mechanical fault detection.

At the foundation of the wavelet transform are wavelet functions obtained by scaling and shifting a function called the mother wavelet. The Continuous Wavelet Transform (CWT) is defined as shown in Equation (7).

$$W(a,b) = \int_{-\infty}^{\infty} x(t)\psi_{a,b}^*(t)dt \tag{7}$$

Here, $x(t)$ represents the analyzed signal, and $\psi_{a,b}^*$ denotes the complex conjugate of the mother wavelet

function created with scale (a) and shift (b) parameters. The mother wavelet function is obtained by scaling and shifting as shown in Equation (8).

$$\psi_{a,b}(t) = \frac{1}{\sqrt{|a|}}\psi(\frac{t-b}{a}) \tag{8}$$

Here, the scale parameter a controls frequency resolution, while b controls the shift on the time axis. Small a values enable the analysis of high-frequency components, while large values enable the analysis of low-frequency components.

In practical applications, the Discrete Wavelet Transform (DWT) is widely used. DWT is obtained by sampling the signal at specific scale and shift values and is defined as shown in Equation (9).

$$W_{j,k} = \sum_n x[n]\psi_{j,k}[n] \tag{9}$$

Here, $x[n]$ represents the discrete-time signal, and $\psi_{j,k}[n]$ represents the discrete wavelet function created with scale j and shift k parameters. In practice, DWT enables the decomposition of the signal into components at multiple resolutions by iteratively passing it through low-pass $h[n]$ and high-pass $g[n]$ filters. The approximation and detail coefficients obtained at each step are calculated as shown in Equations (10.a) and (10.b).

$$A_{j+1}[n] = \sum_l h[k]A_j[2n-k] \tag{10.a}$$

$$D_{j+1}[n] = \sum_l g[k]A_j[2n-k] \tag{10.b}$$

In this process, the coefficients obtained at each level are derived by downsampling, which reduces the signal length by half. Thus, the low-frequency (approximation) and high-frequency (detail) components of the signal are decomposed at each level. The flow diagram showing three levels of WD and the downsampling process is presented in Figure 3. This figure visually summarizes how the signal is decomposed at each level and how the sampling rate decreases.

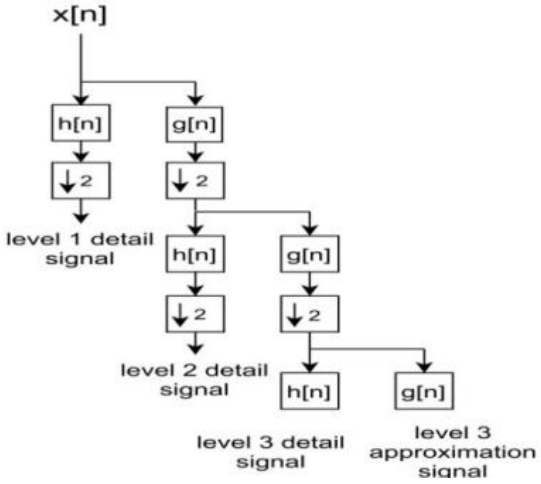

Figure 3 Wavelet decomposition and the downsampling process for 3 levels

2.4 Feature Extraction and Classification

Feature extraction is the process of deriving meaningful and representative attributes from raw data. This process directly impacts model performance in machine learning and data analytics. Time-domain feature extraction is critical for capturing time-dependent dynamics and patterns in the data, because information such as trends, periodicity, and transient changes in time series increases the predictive power of the model.

In this paper, the focus is on specific feature extraction approaches that stand out in the time domain.
In this study, time-domain features were extracted from sub-frequency component signals obtained through both the wavelet transform and EMD methods. Each sub-frequency component was divided into windows of 1s length, and for each window, features such as Mean Absolute Value, Energy, Waveform Length, Willison Amplitude, Zero Crossing, Slope Sign Change, Root Mean Square, Mean, Variance, Standard Deviation, Skewness, and Kurtosis were extracted. With the average of the features extracted for each window, 12 features were extracted for each sub-frequency component. The final feature vector was obtained by combining the features extracted for all sub-frequency components. Figure 4 shows the feature extraction process for each experimental recording.

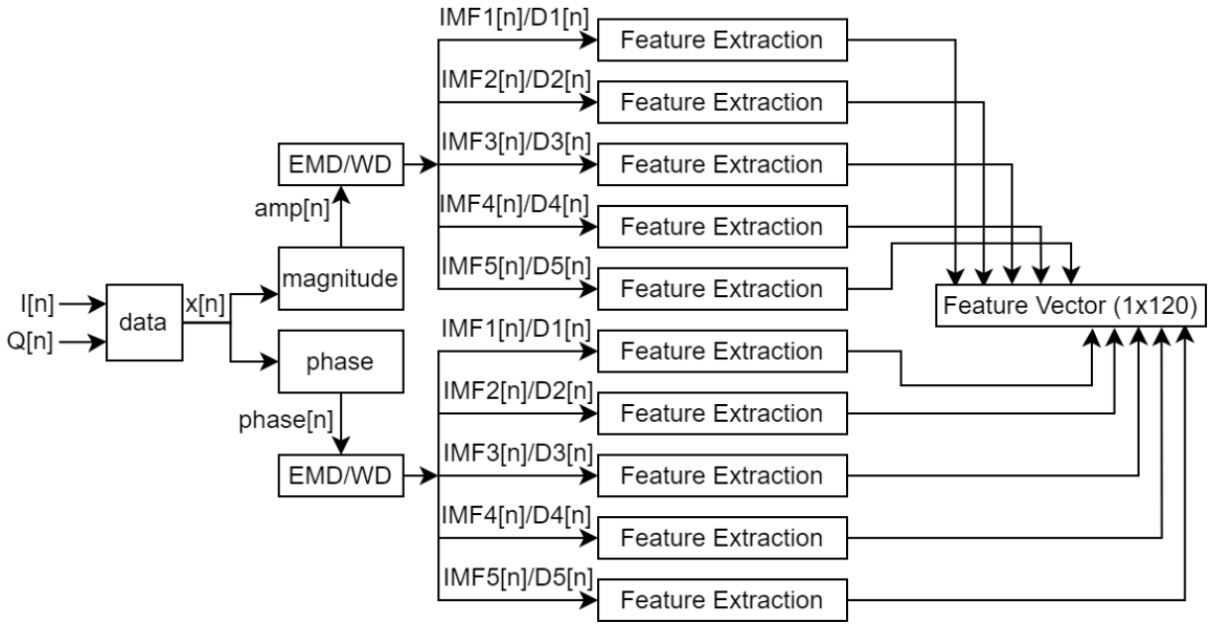

Figure 4 feature extraction process

As illustrated in Figure 4, the feature extraction pipeline systematically processes raw radar signals $I[n]$ and $Q[n]$ obtained from each experimental trial. Initially, these signals are transformed into their corresponding phase ($\phi[n]$) and amplitude ($A[n]$) representations. Subsequently, both phase and amplitude signals are subjected to multi-resolution decomposition through either EMD or WD techniques, resulting in five distinct sub-components for each signal type. Each sub-component is then partitioned into 1-second temporal windows (with an overlapping ration of %50). From each window, twelve time-domain features are extracted. To obtain a representative feature set for each sub-component, the extracted features from all windows are averaged, producing twelve consolidated features per sub-component. The final feature vector is constructed by concatenating features from all sub-components for both EMD and WD approaches. The resulting dataset contains 1,802 experimental samples with a dimensionality of 1,802×121, where the additional column represents the target classification labels corresponding to different imbalance severity levels: 0 indicates balanced condition, 1 denotes mild imbalance, 2 represents moderate imbalance, and 3 signifies severe imbalance. The created data matrix was tested with each of the widely accepted machine learning methods: SVM, KNN, RF, and DT.

2.5 Parameters and Evaluation Metrics

The dataset is divided into training (80%) and testing (20%) sets, employing 5-fold cross-validation for model evaluation. Each machine learning algorithm required specific hyperparameter tuning, which we

accomplished through grid search optimization. This systematic approach evaluated various parameter combinations based on both preliminary experiments and literature recommendations, balancing comprehensive coverage with computational efficiency. Table 3 details the specific hyperparameter search ranges explored for each classifier.

Table 3 Hyperparameter Search Ranges for Classifiers

Method	Parameters
SVM	Kernel function: {'linear', 'rbf', 'polynomial'},C (regularization):{ 0.1, 1, 10, 100}, γ (kernel coef.): {0.001, 0.01, 0.1, 1}
KNN	Num. of neighbor: {1, 10, 50, 100}. Distance metric: {'euclidean', 'cityblock', 'cosine', 'correlation'}.
RF	Number of trees: {50, 100, 200, 300}, Min leaf size: {1, 5, 10}, num. of predictors to sample: {'all', 'sqrt', 'log2'}
DT	MinLeafSize:{1, 5, 10, 20}, maxNumSplits={10, 50, 100, 500}, splitCriter.= {'gdi', 'deviance'}.

The classifier is validated using 5-fold cross-validation across multiple parameter combinations, selecting final models based on the highest average F1 score across all folds.

Performance assessment relied on confusion matrix-derived metrics. This matrix displays classification accuracy for each class in tabular form, showing true positives (correctly identified positive cases), false positives (negative cases incorrectly labeled positive), and false negatives (positive cases incorrectly labeled negative). Equations (11)-(14) present the key performance metrics calculated from these values. Figure 5 illustrates the confusion matrix structure for our four-class classification problem.

$$Accuracy = (\Sigma\ TPs) / (All\ predictions) \quad (11)$$

$$Precision = TP / (TP + FP) \quad (12)$$

$$Recall = TP / (TP + FN) \quad (13)$$

$$F1\ score = 2\ x\ (Precision\ x\ Recall) / (Precision + Recall) \quad (14)$$

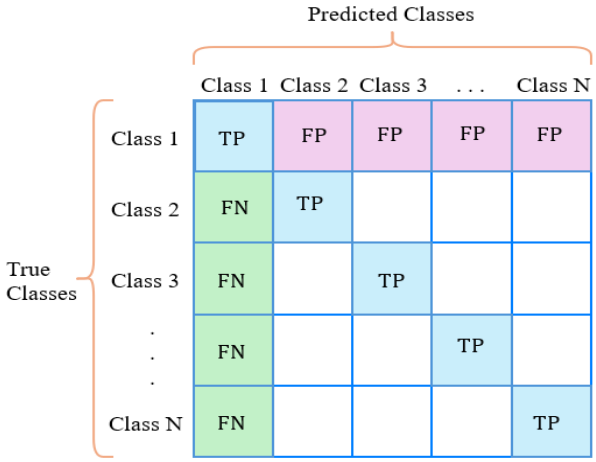

Figure 5 Confusion matrix for a four-class problem

3. Results and Discussion

The experimental evaluation assesses the performance of multi-resolution approaches, specifically WD and EMD, for the radar-based estimation of rotational imbalance level. Each method generated five decomposition signals to extract time-domain features. Then, these features are tested in four different machine learning algorithms: SVM, KNN, RF, and DT. The performances of WD for different wavelet functions and EMD are tabulated in Table 4-7.

Table 4 Performance Comparison for ML algorithms with EMD features

Model Name	Parameters	Acc. (%)	Prec. (%)	Recall (%)	F1 score (%)	Train. time (ms)	Pred. time (ms)	Model size (MB)
SVM	C=10, gamma=0.01, kernel=rbf, polynomialOrder=2.	88.90	88.82	88.79	88.77	127.02	19.61	2.58
KNN	k=1, distance=cityblock.	88.34	88.37	88.23	88.23	10.65	26.47	1.11
RF	numTrees=200, minLeafSize=1, numPredictors=sqrt.	91.12	91.17	91.06	91.08	2628.43	272.51	12.11
DT	minLeafSize=1, maxNumSplits=100, splitCriter.=deviance.	73.14	73.39	72.93	73.02	211.04	0.63	1.14

Table 4 shows that EMD paired with RF (EMD-RF) achieved the highest accuracy, 91.12%, using optimal settings (numTrees=200, minLeafSize=1, numPredictors=sqrt). SVM followed at 88.90% with an RBF kernel (C=10, γ=0.01), KNN was close at 88.34%, and DT lagged at 73.14%. Regarding training speed, KNN was the quickest at 10.65 ms, while RF required much longer training time (2628.43 ms).

Table 5 Performance Comparison for ML algorithms with Haar features

Model Name	Parameters	Acc. (%)	Prec. (%)	Recall (%)	F1 Score (%)	Train. time (ms)	Pred. time (ms)	Model size (MB)
SVM	C=0.1, gamma=1, kernel=polynomial, polynomialOrder=2.	91.74	91.65	91.61	91.61	218.53	13.48	2.21
KNN	k=1, distance=cityblock.	87.72	87.98	87.76	87.74	10.34	26.13	1.11
RF	numTrees=300, minLeafSize=1, numPredictors=sqrt.	95.28	95.28	95.23	95.22	3904.64	401.02	15.55
DT	minLeafSize=1, maxNumSplits=500, splitCriter.=gdi.	84.46	84.59	84.32	84.36	127.41	0.59	1.13

According to Table 5, the RF-Haar combination with 300 trees achieved the highest accuracy at 95.28%, leading the experiments, while SVM with a polynomial kernel (C=0.1, γ=1, degree=2) also performed strongly with 91.74% accuracy, indicating non-linear kernels work well with Haar-derived features. Even the weakest model, DT, reached an accuracy of 84.46%, highlighting the superior discriminative power of Haar features compared with EMD. The primary trade-off is computational cost: RF required 3904.64 ms for training and 401.02 ms for prediction.

Table 6 Performance Comparison for ML algorithms with Coif2 features

Model Name	Parameters	Acc. (%)	Prec. (%)	Recall (%)	F1 Score (%)	Train. time (ms)	Pred. time (ms)	Model size (MB)
SVM	C=10, gamma=0.01, kernel=rbf, polynomialOrder=3.	87.44	87.74	87.33	87.37	159.21	22.41	2.95
KNN	k=1, distance=cityblock.	86.40	86.58	86.43	86.37	10.92	26.57	1.11
RF	numTrees=100, minLeafSize=1, numPredictors=sqrt.	93.20	93.24	93.20	93.17	1322.11	139.25	5.96
DT	minLeafSize=1, maxNumSplits=100, splitCriter.=deviance.	85.22	85.35	85.14	85.10	180.52	0.56	1.13

Table 6 indicates that the Coiflet2 wavelet demonstrated robust and consistent classification performance. Random Forest achieved 93.20% accuracy using 100 trees, while SVM with RBF kernel yielded 87.44% accuracy. KNN and Decision Tree achieved 86.40% and 85.22%, respectively. Table 6 also presents that Coiflet2 offered a better computational trade-off than Haar, with RF training time reduced to 1322.11 ms while maintaining high classification accuracy.

Table 7 Performance Comparison for ML algorithms with Symlet4 features

Model Name	Parameters	Acc. (%)	Prec. (%)	Recall (%)	F1 Score (%)	Train. time (ms)	Pred. time (ms)	Model size (MB)
SVM	C=10, gamma=0.01, kernel=rbf, polynomialOrder=2.	86.54	86.69	86.42	86.43	160.83	22.37	2.94
KNN	k=1, distance=cityblock.	85.64	85.78	85.73	85.64	10.88	26.60	1.11
RF	numTrees=100, minLeafSize=1, numPredictors=sqrt.	93.55	93.60	93.51	93.51	957.20	143.22	6.60
DT	minLeafSize=1, maxNumSplits=100, splitCriter.=deviance.	83.07	83.40	82.96	83.00	126.55	0.63	1.13

Table 7 shows that Symlet4 wavelet features also produced competitive results, with Random Forest achieving 93.55% accuracy. The performance hierarchy remained consistent with other wavelet methods, following the pattern RF > SVM > KNN > DT. Notably, Symlet4 provided the most efficient RF training time (957.20 ms) among all methods while maintaining high classification performance. This consistency across wavelet types indicates the general superiority of wavelet-based feature extraction for this application domain.

Computational efficiency analysis across Tables 4-7 revealed significant variations in training and prediction times. KNN consistently demonstrated the fastest training times (10.34-10.92 ms) across all feature types due to its lazy learning nature. DT algorithms achieved the fastest inference speeds (0.56-0.63 ms), while RF showed the highest prediction latency. Model size analysis indicated that KNN and DT produced the most compact models (~1.11-1.14 MB), while RF models exhibited the poorest memory footprint, ranging from 5.96 MB (Coiflet2) to 15.55 MB (Haar).

Statistical analysis of the experimental results demonstrates the clear superiority of wavelet-based approaches over EMD, with mean accuracies of 89.80% (Haar), 88.07% (Coiflet2), 87.20% (Symlet4), and 85.38% (EMD). RF emerged as the most effective classification algorithm across all feature extraction methods, achieving a mean F1-score of 93.25% ± 1.74%. The comprehensive performance comparison detailed in Table 4-7 is summarized in Figure 6. Figure 6 illustrates the accuracies and the model sizes with a bar chart, while comparing the timing performances with heat maps.

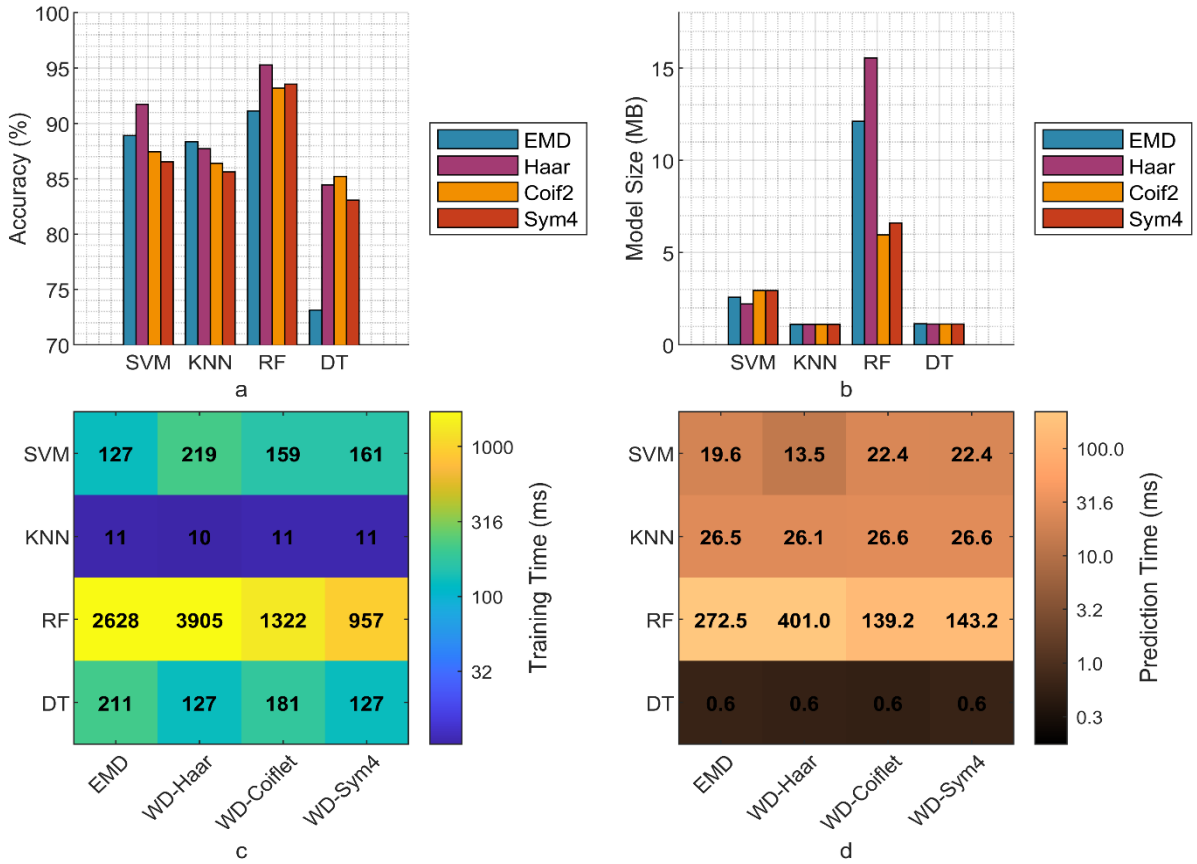

Figure 6 Performance Analysis Summary for All Methods

4. Conclusions

This study demonstrates the effectiveness of radar-based imbalance detection with multi-resolutional analysis (EMD and WD) and machine learning classifiers. The comparative analysis revealed that WD consistently outperformed EMD in feature extraction, with the Haar-RF combination achieving peak accuracy of 95.28% due to WD's robustness against mode-mixing issues inherent in EMD. Among classifiers, RF delivered the highest average accuracy (93.25% ± 1.74%) but required significant computational resources (training up to 3904 ms, model size 15.55 MB), whereas DT provided ultra-fast inference (0.6 ms) and compact models (~1.13 MB) – optimal for edge deployment despite lower accuracy (73–85%). The SVM-Haar pairing offered a balanced compromise (91.74% accuracy, 219 ms training). Therefore, for industrial vibration monitoring, Haar wavelets emerge as the definitive feature extractor. Choose Random Forest for systems demanding peak accuracy, and opt for Decision Trees when ultra-low latency and compact size are paramount for edge deployment.

Although operating speed, load, and imbalance mass were varied to encompass diverse conditions, future work will extend experimental validation to additional motor types, a broader range of power ratings, and various mechanical coupling and mounting configurations to increase generalizability.

Declaration of Ethical Standards

As the authors of this study, we declare that he complies with all ethical standards.

Declaration of Competing Interest

The authors declared that they have no conflict of interest.

Funding / Acknowledgements

The authors received no financial support for this research

Data Availability

The datasets analyzed during the current study are publicly available in the KAGGLE (Acar, 2025).

References

Acar, Y. E., Seflek, I., & Yaldız, E. (2019). Wavelet based denoising of the simulated chest wall motion detected by SFCW radar. Advanced Electromagnetics, 8(2), 85-91.

Acar, Y. E. (2025). Radar Data for Rotational Mass Imbalance Detection Version V0). https://www.kaggle.com/datasets/yunusemreacar1/radar-data-for-machine-fault-detection

Acar, Y. E., & Çetinkal, S. B. (2025). Contactless Detection of Electrical Machine Bearing Faults: A Radar-Based Solution. Black Sea Journal of Engineering and Science, 8(5), 3-4. https://doi.org/10.34248/bsengineering.1673237

Bolshakova, A. V., Boronakhin, A. M., Klionsky, D. M., Larionov, D. Y., Tkachenko, A. N., & Shalymov, R. V. (2023, 25-29 Sept. 2023). Peculiarities of Vibration Signal Processing Techniques Application to Inertial Way Diagnostics. 2023 International Conference on Quality Management, Transport and Information Security, Information Technologies (IT&QM&IS)

Ganguly, P., Chattopadhyay, S., & Datta, T. (2022). Haar-Wavelet-Based Statistical Scanning of Turn Fault in Vehicular Starter Motor. IEEE Sensors Letters, 6(4), 1-4. https://doi.org/10.1109/LSENS.2022.3158608

Glowacz, A., Sulowicz, M., Zielonka, J., Li, Z., Glowacz, W., & Kumar, A. (2025). Acoustic fault diagnosis of three-phase induction motors using smartphone and deep learning. Expert Systems with Applications, 262, 125633

Guo, T., Zhang, T., Lim, E., López-Benítez, M., Ma, F., & Yu, L. (2022). A Review of Wavelet Analysis and Its Applications: Challenges and Opportunities. IEEE Access, 10, 58869-58903. https://doi.org/10.1109/ACCESS.2022.3179517

Han, T., Gong, J. C., Yang, X. Q., & An, L. Z. (2022). Fault Diagnosis of Rolling Bearings Using Dual-Tree Complex Wavelet Packet Transform and Time-Shifted Multiscale Range Entropy. IEEE Access, 10, 59308-59326. https://doi.org/10.1109/ACCESS.2022.3180338

Huang, N. E., Shen, Z., Long, S. R., Wu, M. C., Shih, H. H., Zheng, Q., Yen, N.-C., Tung, C. C., & Liu, H. H. (1998). The empirical mode decomposition and the Hilbert spectrum for nonlinear and non-stationary time series analysis. Proceedings of the Royal Society of London. Series A: mathematical, physical and engineering sciences, 454(1971), 903-995.

Jaarsveldt, C. v., Peters, G. W., Ames, M., & Chantler, M. (2023). Tutorial on Empirical Mode Decomposition: Basis Decomposition and Frequency Adaptive Graduation in Non-Stationary Time Series. IEEE Access, 11, 94442-94478. https://doi.org/10.1109/ACCESS.2023.3307628

Jiang, G., Zhao, J., Jia, C., He, Q., Xie, P., & Meng, Z. (2019). Intelligent fault diagnosis of gearbox based on vibration and current signals: A multimodal deep learning approach. 2019 Prognostics and System Health Management Conference (PHM-Qingdao).

Jiang, P., Chang, Y., Cong, H., & Feng, F. (2020). Nonconvex Wavelet Thresholding Total Variation Denoising Method for Planetary Gearbox Fault Diagnosis. IEEE Access, 8, 78753-78763. https://doi.org/10.1109/ACCESS.2020.2988467

Kiliç, M. E., & Acar, Y. E. (2024). Performance Evaluation of the Time-Frequency Transformation Methods on Electrical Machinery Fault Detection. Bitlis Eren Üniversitesi Fen Bilimleri Dergisi, 13(4), 1147-1157.

Kiranyaz, S., Devecioglu, O. C., Alhams, A., Sassi, S., Ince, T., Avci, O., & Gabbouj, M. (2024). Exploring Sound vs Vibration for Robust Fault Detection on Rotating Machinery. IEEE Sensors Journal.

Li, Y., Zhou, J., Li, H., Meng, G., & Bian, J. (2023). A Fast and Adaptive Empirical Mode Decomposition Method and Its Application in Rolling Bearing Fault Diagnosis. IEEE Sensors Journal, 23(1), 567-576. https://doi.org/10.1109/JSEN.2022.3223980

Manhertz, G., & Bereczky, A. (2021). STFT spectrogram based hybrid evaluation method for rotating machine transient vibration analysis. Mechanical Systems and Signal Processing, 154, 107583. https://doi.org/https://doi.org/10.1016/j.ymssp.2020.107583

Matania, O., Dattner, I., Bortman, J., Kenett, R. S., & Parmet, Y. (2024). A systematic literature review of deep learning for vibration-based fault diagnosis of critical rotating machinery: Limitations and challenges. Journal of Sound and Vibration, 590, 118562. https://doi.org/https://doi.org/10.1016/j.jsv.2024.118562

Piritech Electric Vehicle and Automation Systems. (n.d.). *Asynchronous motor*. Retrieved August 1, 2025, from https://piritechnology.com/asenkron-motor/

Ren, Z., Xiong, Y., Peng, Z., & Meng, G. (2023). 3D microwave vibrometer: Contactless three-dimensional vibration measurements using microwave radars. Mechanical Systems and Signal Processing, 183, 109622. https://doi.org/https://doi.org/10.1016/j.ymssp.2022.109622

Seid Ahmed, Y., Abubakar, A. A., Arif, A. F. M., & Al-Badour, F. A. (2025). Advances in fault detection techniques for automated manufacturing systems in industry 4.0 [Review]. Frontiers in Mechanical Engineering, Volume 11 - 2025. https://doi.org/10.3389/fmech.2025.1564846

Stallone, A., Cicone, A., & Materassi, M. (2020). New insights and best practices for the successful use of Empirical Mode Decomposition, Iterative Filtering and derived algorithms. Scientific Reports, 10(1), 15161. https://doi.org/10.1038/s41598-020-72193-2

Şeflek, İ. (2025). Empirical Mode Decomposition for Power Spectral Density Features in Radar-Based Fall Detection. Erciyes Üniversitesi Fen Bilimleri Enstitüsü Fen Bilimleri Dergisi, 41(1), 318-330. https://dergipark.org.tr/tr/pub/erciyesfen/issue/91637/1650238

Tama, B. A., Vania, M., Lee, S., & Lim, S. (2023). Recent advances in the application of deep learning for fault diagnosis of rotating machinery using vibration signals. Artificial Intelligence Review, 56(5), 4667-4709. https://doi.org/10.1007/s10462-022-10293-3

Vaishnavi, N., Mansha, A., Samarth, K., Honey, K., & Vishnu Vijay, K. (2025, 2025/07/01). Structural Health Monitoring in Aerospace: Integrating Sensor Technologies for Enhanced Safety and Efficiency. Proceedings of the 10th International Conference on Science and Technology (ICST 2024),

Wen, R., Zhang, D., Chen, J., & Sun, Q. (2024). Contactless Micron-Level Vibration Measurement with Millimeter Wave Radar. APSIPA Transactions on Signal and Information Processing, 13(4).

Wu, J., & Yang, C. (2025). Time–frequency extracting transform and its applications in vibration signal processing. Measurement, 243, 116284. https://doi.org/https://doi.org/10.1016/j.measurement.2024.116284

Ye, Z., Hsu, S.-C., & Wei, H.-H. (2022). Real-time prediction of structural fire responses: A finite element-based machine-learning approach. Automation in Construction, 136, 104165. https://doi.org/https://doi.org/10.1016/j.autcon.2022.104165

Yücel, E., Karabulut, C., & Çunkaş, M. (2025). Design, implementation, and testing of a propulsion system for the hyperloop transportation system. Electrical Engineering. https://doi.org/10.1007/s00202-025-03107-6

Zheng, J., Cao, S., Feng, K., & Liu, Q. (2024). Zero-Phase Filter-Based Adaptive Fourier Decomposition and Its Application to Fault Diagnosis of Rolling Bearing. IEEE Transactions on Instrumentation and Measurement, 73, 1-11. https://doi.org/10.1109/TIM.2022.3228005